

Adhesion of the electrodes on diamond device surfaces

Tom Ichibha^{1,*}, Kenta Hongo^{2,3,4}, I. Motochi⁵, N. W. Makau⁶, G. O. Amolo⁷, and Ryo Maezono²

¹School of Materials Science, JAIST, Nomi, Ishikawa, Japan

²School of Information Science, JAIST, Nomi, Ishikawa, Japan

³National Institute of Materials Science, Tsukuba, Ibaraki, Japan

⁴PRESTO, JST, Kawaguchi, Saitama, Japan

⁵Department of Mathematics and Physical Sciences, Maasai Mara University, Narok, Kenya

⁶Computational Materials Science Group, Department of Physics, University of Eldoret, Eldoret, Kenya

⁷Department of Physics and Space Science, The Technical University of Kenya, Nairobi, Kenya

*ichibha@icloud.com

ABSTRACT

Appropriate candidates of the metallic sheet used for the electrodes of diamond semiconductor are investigated using computational approaches based on density functional theory (DFT). For twenty kinds of metallic elements x , we modeled a diamond-metal interface and evaluated its work of separation, $W_{\text{sep}}(x)$, as a possible measure of anti-peeling strength. The appropriateness of the Ohmic contact was inferred from DOS (density of states) analysis of diamond-metal interface by looking at whether an in-gap (isolated/localized) peak disappears as well as a sufficient amount of DOS value exists around the Fermi level. Our DFT simulation confirmed that a typical electrode, Au, is not adhesive enough for power devices [$W_{\text{sep}}(\text{Au}) = 0.80 \text{ J/m}^2$], though showing the Ohmic contact. In contrast, some transition metals were found to possess Ohmic features with much stronger adhesion than Au [e.g., $W_{\text{sep}}(\text{Cr/Ti}) = 6.02/4.03 \text{ J/m}^2$].

1 Introduction

Diamond is a promising candidate for the next-generation power devices, possessing a wider band gap by a factor of five and a higher thermal conductivity by a factor of more than ten,¹ compared with Si.^{2,3} These properties are key for the device robustness in its anti-voltage and anti-thermal strengths which is required especially in power semi-conductor devices. Its higher electron mobility, 1.3 times or more faster than Si, makes the device a very good candidate for use in signal processing with higher frequencies.

Chemical vapor deposition (CVD) has enabled industrial synthesis of diamond for devices,^{4,5} leading to the recent feasibility to obtain larger single crystals with higher purity.⁶ Doping techniques to establish the junctions have also been studied intensively both from theory and experiments.⁶ The p -type doping has been well developed and Metal-insulator semiconductor field-effect transistor (MISFET) has been realized on the films by homo epitaxial growth.⁷ Diamond junction FET have indeed been confirmed to work very well.⁸ In contrast, the n -type doping has been difficult to realize, but its synthesis has recently been reported.⁹ The feasibility for device fabrication is now quite real thereby leaving the matter of the realization of $n+$ layer in the doping challenges.

Another important issue is the electrode fabrication, namely the Ohmic contact of the metallic layer on the diamond surface. There are several experimental attempts that have been made, mainly using Au because of its low contact resistance.¹⁰⁻¹² For p -type doped diamonds the electrode fabrication has been well established as reported.¹³ Although diamond surfaces are naturally clean, *i.e.*, not terminated with either hydrogen or oxygen, the possible varieties of the surface terminations and the dependence of the electrode properties on the termination elements are of great interest to researchers.^{11,12,14-17} For instance, it is experimentally reported that diamond surface-channel FET's on hydrogen-terminated surface would be promising candidates for some power applications.¹² Other metallic elements especially Al, Au/Ti, and Al/Ti, have systematically been investigated to establish if they form better electrodes on the hydrogen-terminated p -type diamonds fabricated by CVD.¹¹ Besides typical electrode metals such as Au and Pd, both Ti and Mo have been used for electrode fabrications and their specific contact resistance has been measured experimentally¹¹ using circular transfer length method (c-TLM).¹⁰

In order to realize diamond power devices, it is quite important to establish how to fabricate such electrodes that possess not only low contact resistance¹⁰, but also high adhesion to the surface. This is essential for establishing anti-peeling strength under high voltage and temperature that may occur in power devices.²

A number of theoretical works have treated the adhesion between diamond surface and several metals,^{18–28} but their exploration space were limited as shown here and hence there still exist the possibilities of discovering more appropriate electrode metals for diamond surfaces. Pickett and Erwin^{18,20} were among the first to investigate metal/diamond interfaces for electronic device applications using first-principles local-density functional approaches, followed by the pioneering work on BN/diamond interfaces by Lambrecht and Segall.¹⁹ They modeled nickel/diamond interfaces on both the (001) and (111) ideal surfaces and computed their Schottky barrier heights and interface energies. It was found that the tetrahedral arrangement leads to an Ohmic interface with the interface energy of 0.97 eV per carbon atom, suggesting that the interface geometry plays a crucial role in its surface electronic structure. Afterward, the Ohmic properties were verified by an experimental work²⁹ to support the above theory-driven prediction.

Recent works^{25–28} examined material structure model and studied several metals. Guo *et al.*²⁵ treated 3 metals (Al, Cu, Ti) on clean diamond (111)-(1 × 1) surface. Monachon *et al.*²⁸ treated 2 metals (Cu, Ni) on clean and hydrogen terminated diamond (111)-(1 × 1) surfaces. These two works evaluated the adhesion by the work of separation (W_{sep}), and they treated the model of metallic electrodes as multi-layer: The work of separation represents the adhesion between metal and diamond bulks.

On the other hand, Motochi *et al.*²⁶ modeled the interfaces as periodic slabs comprised of monolayer metallic electrodes and ten-layer diamond surfaces with/without monolayer atomic terminations. They applied density functional theory (DFT) approaches to evaluate adsorption energy, E_{ads} and density of states (DOS) for their target systems. They concluded that tantalum and vanadium were the best metallic electrodes because they showed highest E_{ads} with surface metallic properties, *i.e.* the localized surface electronic state, after the adhesion.

In this study we revisit the previous work by Motochi *et al.*²⁶ because of the following points. Although their work was a challenge and gave a great insight to the possibility of the carbide forming metals to form better electrodes, their computations and metals considered were limited. In contrast, the present study has systematically explored a broad range of metals for more desirable diamond electrodes. We considered twenty types of elements: Mg, Al, Ti, V, Cr, Ni, Cu, Zn, Zr, Nb, Mo, Pd, Ag, In, Hf, Ta, W, Pt, Au, and Pb. Here we adopted the same metal/diamond structure model as that by Motochi *et al.*,²⁶ but paid more careful attention to the evaluation of adhesion for which we employed W_{sep} instead of E_{ads} . This is because E_{ads} is inappropriate for our purpose as discussed later. Our more extensive exploration with great care has led us to a different conclusion from that of Motochi *et al.*²⁶ in terms of the best choice for metallic electrode.

In this section we have reviewed previous studies on the diamond surfaces and made a brief explanation of our findings. The following sections are organized as follows: §2 presents the surface models and methodology. In §3, the results of the work are presented and finally the conclusions drawn from the findings are given in §4.

2 Model and Methodology

Fig. 1 shows our slab model of interfaces between metallic electrodes and diamond (111)-(1 × 1) surfaces with/without terminations (H and O), which is the same as that in the previous work by Motochi *et al.*²⁶ We considered the 20 metals and three terminations and hence a total of 60 interface systems in order to explore desirable electrodes for power device applications. We have performed DFT calculations with carefully chosen computational conditions (shown later) and optimized the geometries using QUANTUM ESPRESSO³⁰ with PBE-GGA³¹ exchange-correlation XC functional and ultrasoft pseudo potentials³² available therein. Most of the preceding works have taken W_{sep} as the measure of adhesion strength,^{21–23,25,28} which excludes the energy gain due to the cohesion of the metallic sheet itself unlike W_{ads} .²⁶ Thus, we also adopted W_{sep} to evaluate the adhesion strength. We have verified whether or not our model can accurately simulate the interfaces in terms of partial density of states (pDOS) at each of the diamond layers, which was not investigated in the previous study.²⁶

We define the work of separation:

$$W_{\text{sep}}(x) = \frac{1}{2\Omega} (E_{\text{parent_surface}} + 2 \cdot E_{\text{sheet}}(x) - E_{\text{slab}}(x)). \quad (1)$$

Here, Ω is the surface area of unit cell, (i) $E_{\text{parent_surface}}$ is the energy per unit cell of the diamond slab with/without termination (parent surface), (ii) $E_{\text{slab}}(x)$ is the energy of the whole interface system (slab) with the sheets of metal x , and (iii) $E_{\text{sheet}}(x)$ is the energy of the sheet of metal x (electrode). The factor 1/2 in eq. (1) comes from the fact that our slab model has interfaces on both sides.

Within the framework of the DFT approaches, all the three energies (i), (ii), and (iii) were computed under the conditions that $E_{\text{cut}}^{\text{wfc}} = 90$ Ry for the cutoff energy of the orbital function expansion and $E_{\text{cut}}^{\text{rho}} = 520$ Ry to compensate charges in the ultrasoft pseudo-potential evaluation. The k -mesh size (discretization of Brillouin zone) of $14 \times 14 \times 1$ was used for all the

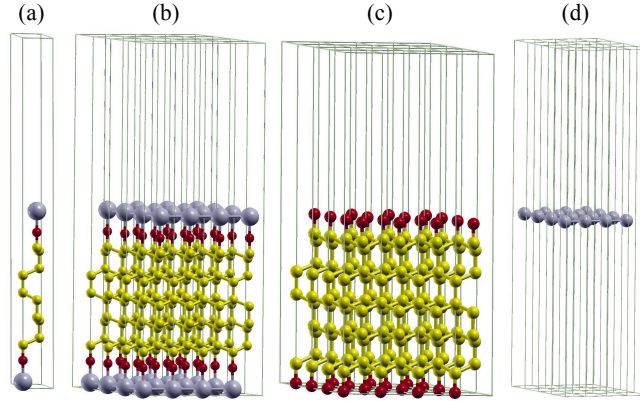


Figure 1. Interface models: (a) unit cell of slab, (b) $4 \times 3 \times 1$ supercells of slab, (c) parent surface (with terminations), and (d) metallic electrode. The large, small (dark), and small (light color) balls correspond to the metal, terminating atoms (hydrogen or oxygen), and carbon atoms, respectively.

three energies. The Marzari-Vanderbilt smearing scheme³³ with $\delta E = 0.02$ Ry was applied to all the systems. The above computational specifications were the best choices for all the systems, but they were also very carefully chosen such that all the evaluations of interface energy lie within the chemical accuracy of ~ 2 mRy/unit cell. Hereafter we describe how to model the metal-(terminating atom)-diamond interface system (slab) and its subsystems (parent surface and metal) in order to evaluate the corresponding three energies in more detail.

First, we extracted a ten-layer diamond slab with an ideal (111)- (1×1) surface from the bulk structure. As confirmed later in § 3.1, the number of layers is sufficiently large to capture the change in the electronic structure from surface to bulk inside. To construct the diamond surface, we chose a vacuum phase with dimension of 9.2 \AA subject to the periodic boundary condition, which means that the upper and lower five layers are identical. In order to take into account surface reconstructions, we optimized both the atomic positions and lattice parameters (i.e., unit cell size) simultaneously within the PBE-GGA method under the above condition. Our resulting optimized geometry reasonably agrees with the experiment³⁴ as well as that by Motochi *et al.*²⁶ The number of the layers (Fig. 1) has been found to be large enough to simulate the (111)- (1×1) surfaces because the geometry at the fifth and sixth layers is almost the same as that of the bulk. The optimized geometry was used to evaluate $E_{\text{parent_surface}}$. Erwin and Pickett³⁵ pointed out that the dangling bonds of the (111)- (1×1) surface are located at on-top sites. In the case of H- and O-terminations, therefore, we placed the terminating atoms at an on-top site of the above optimized (111)- (1×1) surface. Starting with initial atomic configurations separated by their covalent radii,³⁶ we fixed the lattice parameters and reoptimized all the atomic positions and found that both the hydrogen and oxygen terminating atoms stay at the on-top site with only a change in the vertical distance between the surface carbon atom and the terminating atoms.

Secondly, since the on-top site may be thought of as being the most preferable to electrode adhesion, we constructed the slab model by putting metallic monolayers at the on-top site of the optimized (111)- (1×1) surface. Starting with initial atomic configurations separated by their covalent radii, we fixed the lattice parameters and reoptimized all the atomic positions to get $E_{\text{slab}}(x)$. Note that our unit cell contains only one metallic atom on the surface. This means that we ignore lattice mismatches at interfaces, but as discussed later, they were found to be negligible. Similar to the no-termination case, we placed metallic monolayers on the H- or O-terminating diamond surfaces and reoptimized the geometries.

Finally, we considered the metallic monolayers (i.e., two dimensional metallic sheets) without optimizing their geometries, which was used to evaluate $E_{\text{sheet}}(x)$. The errors due to omitting the optimizations are found to be negligible as discussed later in § 3.4. Since all the slab systems are non-magnetic, we treated all the 2D sheets as being paramagnetic, irrespective of their actual magnetic states.³⁷

The DOS analysis gives a useful insight into the Ohmic contact property, especially by investigating whether or not the in-gap peak disappears²⁶ as summarized in Fig. 3. The peak corresponds to the localized surface state forming the Schottky contact rather than the Ohmic contact. The appropriateness for the Ohmic contact is therefore inferred from DOS analysis of metal/diamond interface by checking if the system possesses the larger DOS at E_F (the larger availability for valence electrons) and non-peaky shape of DOS (non-localized property of electrons). In addition, pDOS tells one which angular component

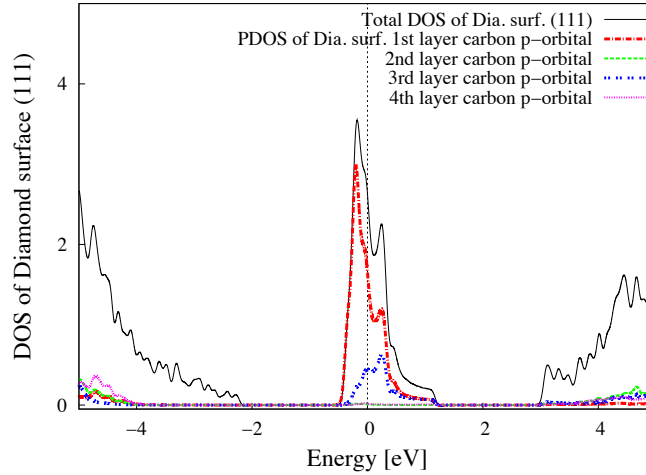


Figure 2. Partial contributions to DOS from each layer of the diamond slab. Only the first three layers contribute mainly to the surface state appearing between the bulk gap. Energy as the horizontal axis is set with the Fermi energy at 0 eV.

contributes mostly to the carrier in the vicinity of the Fermi level. We also evaluated the difference between the DOS of diamond slab and that of the system with electrodes attached in order to understand how charge transfer occurs.

3 Results and discussion

3.1 Number of diamond layers

We have checked if the number of diamond layers is large enough to simulate the interfaces by looking into pDOS contributions at each diamond layer to the total DOS, as shown in Fig. 2. It is found that $2p$ orbitals from the first three layers mainly contribute to the surface state appearing within the bulk gap. This corresponds to the fact that any surface reconstruction occurs only within the first two layers. This is consistent with previous studies by Pickett and Erwin.^{20,38} We note in Fig. 2 that the width of the in-gap peak, ~ 2 eV, is a bit wider than that usually expected for the surface state.³⁹

3.2 Density of states

Fig. 3 draws the comparison of DOS among the different kinds of metallic sheets to be examined. Each panel includes the comparison among the kind of terminations (with H, O, and w/o termination). The evaluation for the better electrode performances is made, as explained in §1, based on (1) whether the DOS fills the gap seen for pristine diamond surface in Fig. 2, and (2) how large the DOS is around the Fermi level. 'Ti sheet w/o termination' therefore achieves the best performance in this sense, followed by 'Cr with H-termination', 'Cr w/o termination', 'V with H-termination', 'V w/o termination', 'Cr with O-termination', and 'Ti with O-termination' in this order. In contrast to that, the familiar electrode materials, Au, Pb and Pt, are found to be not necessarily the best choice to form the Ohmic contact: For Au and Pt, the DOS filling on the gap is relatively small. Pb achieves acceptable filling but the DOS around E_F is relatively small. Though the largest DOS around E_F is achieved by Ni sheet in a peaky shape, it cannot fill the gap well, corresponding to the formation of the localized surface state.

Peaky shape of DOS near to E_F in Fig. 3, appearing for Ti, Cu, Pd, In, Ta, Pt, Mg, V, Ni, Zn, Zr, Ag, Hf, and Au, would be attributed to the in-gap state for the diamond slab, but this could be also interpreted as MIGS (Metal Induced Gap States)^{40,41}: The metallic wavefunction penetrates towards diamond as an evanescent wave at the metal/diamond interface, and the wave builds the interface states called MIGS.^{40,41}

3.3 Bonding natures and adhesion lengths

Fig. 4 shows the change in the bonding lengths during the lattice relaxation starting off the initial value taken as the sum of covalent radii of constituent atoms of the interface. There is a clear contrast to get elongation or contraction of the adhesion lengths after the change between the initial and optimized bond lengths (atomic positions were optimized from their initial ones separated by the covalent radii of atoms constituting the interfaces, as explained in §2). The contrast might be attributed to the different bonding nature, such as ionic or covalent. In the case of no-termination, for instance, Al (Ti) gives elongation (contraction), being consistent with the covalent (ionic) nature of the elements. Significant elongations for the hydrogen

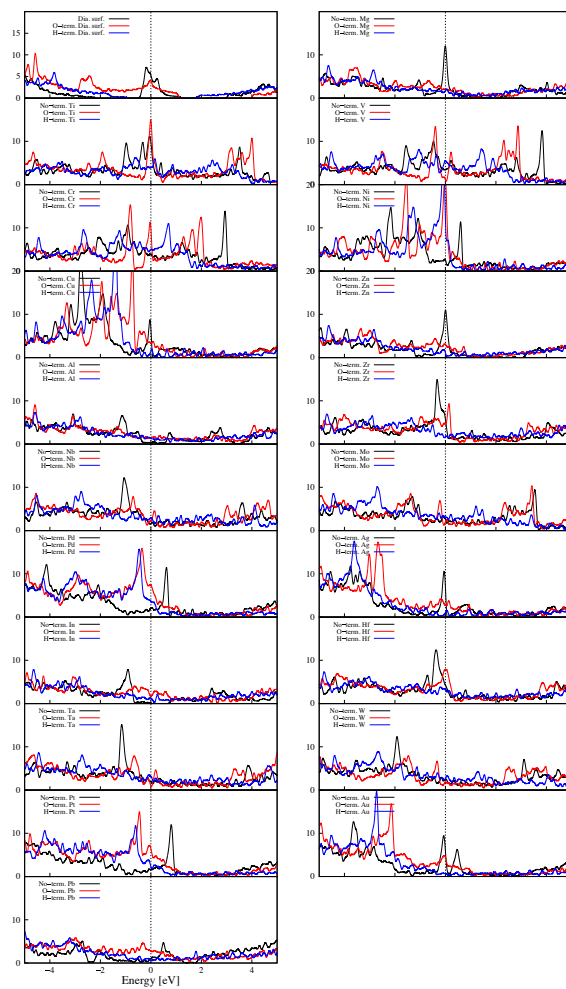


Figure 3. DOS of the parent surface and the metal sheets with Hydrogen, Oxygen, and no terminations. Blue, red, and black lines correspond to Hydrogen, Oxygen, and no terminations respectively. The vertical dotted line represents Fermi energy.

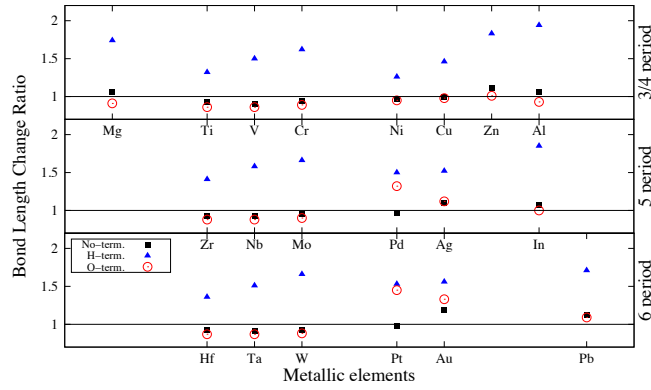


Figure 4. Deviations of the adhesion lengths from the initial values for the geometrical optimizations. The sum of the initial covalent radii is shown to be unity. Open rectangles (closed triangles) correspond to the lengths between the termination elements and metallic elements (surface carbon atoms). No-term. stands for no termination while H-term. and O-term. stand for hydrogen- and oxygen- terminated surfaces respectively.

terminations compared with the oxygen terminations and no-terminations might also be attributed to the fact that the diamond surface has only one dangling bond that hybridizes with the hydrogen $1s$ orbital and then there is no room for additional bonding with the electrode metals. In the case of O-termination, d_{adh} got contracted [elongated] for transition metals (Ti, Ta, V) [noble ones (Au, Pd)]. This contrast can be attributed to whether the d/f orbitals of the valence shell are closed (for noble metals) or not.¹ The trend in the magnitude of the contraction can be explained to some extent in terms of the electronegativity: the more contractions by the elements with the smaller numbering of groups (*i.e.*, left hand side in the periodic table) would be accounted for by the smaller electronegativities. The difference of the negativities between the metallic elements and the top-most atom on the surface (carbon or oxygen) gets larger when the negativity of the metallic element itself gets smaller. The larger difference leads to the ionic bonding nature, and hence to the more contraction. The scenario is consistent with the fact that we get more contractions by O-termination than no-termination because oxygen has the larger electronegativity and hence gives a larger difference of electronegativity.

3.4 Work of separation

Fig. 5 highlights the dependence of $W_{\text{sep}}(x)$ on the metallic elements x and the terminations (no-termination, O- and H-terminations), evaluated from our PBE-GGA simulations with the ultrasoft pseudopotentials. It is found that overall trends in $W_{\text{sep}}(x)$ strongly depends on the termination elements, reflecting their surface bonding natures. In the case of the no-termination, as is expected, the Au electrode has the weakest adhesion. Surprisingly, the Pd is found to have a slightly stronger adhesion than the Ti that forms a carbide. The group-6 elements (Cr, Mo and W) have stronger adhesions than the other elements. For any metal, the H-termination hinders the metal from forming the electrodes because of weak bonding (see §3.3). In contrast, the O-termination makes quite different effects on the adhesion. It weakens the adhesion for the noble metals (Au, Ag, Pt, and Pd), while it significantly strengthens for some transition metals (group-4,5,6) by enhancing the ionic natures of bonding (see §3.3). O-terminated Cr and Ti are the promising candidates to achieve both higher DOS at the Fermi level, $D(\epsilon_F)$, and anti-peeling strength. It is remarkable that W_{sep} for O-terminated Cr is around twice larger than that for no-terminated Ti. Comparing W_{sep} between no-termination and O-termination, it is interesting to note that W_{sep} increases from group 4 to 6 for no-termination but such a clear tendency does not appear for O-termination. We revealed instead W_{sep} has a negative correlation with adhesion length clearly (Fig. 6).

Table 1 compares our numerical results of W_{sep} and d_{adh} with those by previous studies^{23,25,28} for Ni, Cu, Al, and Ti. Note that our metal/diamond interface models consider only monolayers, while the previous ones do multilayers. Despite such a significant difference, we found that our numerical results for Cu and Ni agree well with the previous ones (their differences in W_{sep} and d_{adh} lie within $\sim 0.6 \text{ J/m}^2$ and $\sim 0.04 \text{ \AA}$, respectively). On the other hand, our work overestimated d_{adh} values for Al and Ti. Interestingly, the overestimation affects W_{sep} in the opposite manner, *i.e.*, W_{sep} increases (decreases) for Al (Ti). This may be explained by the different nature of the bonding, *i.e.*, covalent for Al and ionic for Ti as discussed in § 3.3: Covalent bonds generally tends to have longer bond lengths (*e.g.*, sparse structure in diamond structure) than ionic ones (*e.g.*,

¹For Au, the partially occupied $6s$ orbital can contribute to the bonding with oxygen atoms. However it may be weak because s orbital has a spherical shape and may have less overlap with p orbital of oxygen than d/f orbitals.

Table 1. Comparison of W_{sep} (J/m^2) between ours and literatures for several metals (Al, Cu, Ti, and Ni). The corresponding d_{adh} values (\AA) are also given in parentheses. Note that the present metal/diamond interface models employ monolayer metallic sheets, while the previous ones did multi-layer metallic sheets.

	This work	H. Guo <i>et al.</i> ²⁵	C. Monachon <i>et al.</i> ²⁸	Y. Qi and L.G. Hector ²³
Al	4.90 J/m^2 (2.09 \AA)	4.08 J/m^2 (1.86 \AA)	N/A	3.98 J/m^2 (1.86 \AA)
Cu	2.90 J/m^2 (2.06 \AA)	3.36 J/m^2 (2.09 \AA)	3.04 J/m^2 (N/A)	N/A
Ti	4.04 J/m^2 (2.18 \AA)	5.77 J/m^2 (1.94 \AA)	N/A	N/A
Ni	5.65 J/m^2 (1.92 \AA)	N/A	5.00 J/m^2 (1.96 \AA)	N/A

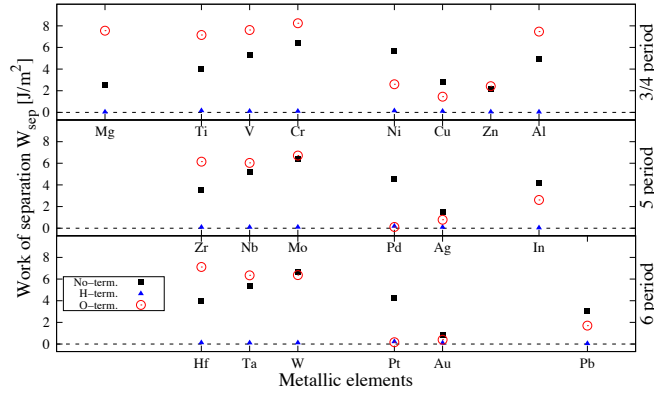


Figure 5. Work of separation W_{sep} obtained from our PBE-GGA simulations with the ultrasoft pseudopotentials. No-term. stands for no-termination while H-term. and O-term. stand for hydrogen- and oxygen- terminated surfaces respectively.

NaCl structure). The optimal adhesion length for Al would be longer than the previous ones and closer to ours, leading to the stronger adhesion. On the other hand, our predicted adhesion length for Ti seems to deviate from the optimal one, leading to the weaker adhesion.

We note that the present work did not take explicitly into account the energy loss/gain by the lattice relaxation. The metallic ion is located just above the carbon atom in our slab model. This corresponds to the situation where the lattice of metallic sheet is forced to have the same lattice constant as the diamond surface. We may estimate the energy loss due to this artificial distortion. From the literature values of bulk modulus of metals, we can roughly estimate the energy loss that arises when the lattice of metallic sheets is distorted towards that of diamond surface. Taking Birch-Murnaghan equation of state,⁴² we estimate the loss being 0.377 J/m^2 for Au, 0.015 J/m^2 for Pd, 0.073 J/m^2 for Ti, 0.342 J/m^2 for V, and 0.078 J/m^2 for Ta. Such energy losses are negligibly small compared with $W_{\text{sep}}(x)$ for metal sheets that show good adhesion.

4 Conclusion

The predicted adhesion energies indicates that the transition metal sheets can be better candidates for the electrodes on the diamond (111) surfaces, realizing more stable adhesion than conventional noble metal electrodes. DOS analysis does indeed confirm that some of those are realizing Ohmic contacts. For the termination atoms of diamond surfaces, hydrogen is predicted to be unbound with metallic sheets while oxygen assists with the realization of more stable adhesion. The trend of the relative adhesion length for covalent length can be reasonably explained in terms of the electronegativity. It is also observed that adhesion strength has a negative correlation with adhesion length. We find that Cr with oxygen-termination achieves the largest adhesion in terms of work of separation, while Ti with no-termination realizes the largest carrier density in terms of DOS at the Fermi level.

5 Acknowledgments

The computations in this work have been performed using the facilities of the Center for Information Science in JAIST. This work was supported by the Kenya National Council for Science and Technology (NCST, Now National Commission for Science, Technology and Innovation (NACOSTI)) Grant No. NCST/5/003/4th CALL/050, and the Computational Materials

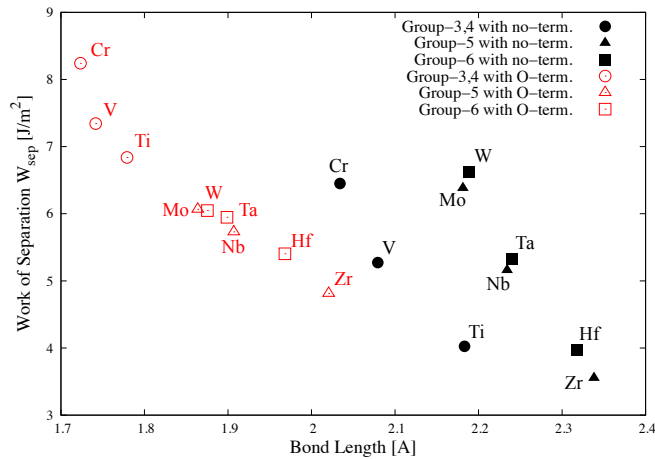


Figure 6. Relationship between adhesion length and work of separation W_{sep} . No-term. stands for no-termination while O-term. stands for oxygen-terminated surface.

Sciences Group, Department of Physics, University of Eldoret, Kenya. Authors, IM, NWM, and GOA wish to acknowledge the Center for High Performance Computing (CHPC) in Cape Town South Africa for computational resources. KH is grateful for financial support from a KAKENHI grant (15K21023, 17K17762), a Grant-in-Aid for Scientific Research on Innovative Areas (16H06439), PRESTO (JPMJPR16NA) and the “Materials research by Information Integration” Initiative (MI²I) project of the Support Program for Starting Up Innovation Hub from Japan Science and Technology Agency (JST). R.M. is grateful for financial support from TOKUYAMA science foundation, MEXT-KAKENHI grants 17H05478, the support by FLAGSHIP2020, MEXT for the computational resources, Project Nos. hp170269 and hp170220 at K-computer.

References

1. Maezono, R., Ma, A., Towler, M. D. & Needs, R. J. Equation of state and raman frequency of diamond from quantum monte carlo simulations. *Phys. Rev. Lett.* **98**, 025701 (2007). URL <https://link.aps.org/doi/10.1103/PhysRevLett.98.025701>.
2. Willander, M., Friesel, M., Wahab, Q. & Straumal, B. Silicon carbide and diamond for high temperature device applications. *J. Mater. Sci. - Mater. Electron.* **17**, 1–25 (2006). URL <http://dx.doi.org/10.1007/s10854-005-5137-4>.
3. Maezono, R., Drummond, N. D., Ma, A. & Needs, R. J. Diamond to β -tin phase transition in si within diffusion quantum monte carlo. *Phys. Rev. B* **82**, 184108 (2010). URL <https://link.aps.org/doi/10.1103/PhysRevB.82.184108>.
4. Matsumoto, S., Sato, Y., Kamo, M. & Setaka, N. Vapor deposition of diamond particles from methane. *Jpn. J. Appl. Phys.* **21**, L183–L185 (1982). URL <http://jjap.jsap.jp/linkJJAP/21/L183/>.
5. Kamo, M., Sato, Y., Matsumoto, S. & Setaka, N. Diamond synthesis from gas phase in microwave plasma. *J. Cryst. Growth* **62**, 642 – 644 (1983). URL <http://www.sciencedirect.com/science/article/pii/0022024883904116>.
6. Mokuno, Y., Chayahara, A., Yamada, H. & Tsubouchi, N. Improvements of crystallinity of single crystal diamond plates produced by lift-off process using ion implantation. *Diamond Relat. Mater.* **19**, 128 – 130 (2010). URL <http://www.sciencedirect.com/science/article/pii/S0925963509002507>.
7. H. Umezawa, S. Y. D. T. H. O. H. K., K. Tsugawa. High-performance diamond metal-semiconductor field-effect transistor with 1m gate length. *Jpn. J. Appl. Phys.* **38**, L1222–L1224 (1999). URL <http://ci.nii.ac.jp/naid/110003921086/>.
8. Iwasaki, T. *et al.* Diamond junction field-effect transistors with selectively grown n+-side gates. *Appl. Phys. Express* **5**, 091301–091301–3 (2012). URL <http://ci.nii.ac.jp/naid/40019425038/>.

9. Kato, H., Yamasaki, S. & Okushi, H. n-type doping of (001)-oriented single-crystalline diamond by phosphorus. *Appl. Phys. Lett.* **86**, 222111 (2005). URL <http://scitation.aip.org/content/aip/journal/apl/86/22/10.1063/1.1944228>.
10. Hewett, C., Taylor, M. J., Zeidler, J. & Geis, M. Specific contact resistance measurements of ohmic contacts to semiconducting diamond. *J. Appl. Phys.* **77**, 755–760 (1995).
11. Looi, H. J., Pang, L. Y., Whitfield, M. D., Foord, J. S. & Jackman, R. B. Engineering low resistance contacts on p-type hydrogenated diamond surfaces. *Diamond Relat. Mater.* **9**, 975 – 981 (2000). URL <http://www.sciencedirect.com/science/article/pii/S0925963500002405>.
12. Gluche, P., Aleksov, A., Vescan, A., Ebert, W. & Kohn, E. Diamond surface-channel fet structure with 200 v breakdown voltage. *IEEE Electron Device Lett.* **18**, 547–549 (1997).
13. Moazed, K. L., Nguyen, R. & Zeidler, J. Ohmic contacts to semiconducting diamond. *IEEE Electron Device Lett.* **9**, 350–351 (1988).
14. Aoki, M. & Kawarada, H. Electric properties of metal/diamond interfaces utilizing hydrogen-terminated surfaces of homoepitaxial diamonds. *Jpn. J. Appl. Phys.* **33**, L708 (1994). URL <http://stacks.iop.org/1347-4065/33/i=5B/a=L708>.
15. Cherian, R., Gerard, C., Mahadevan, P., Cuong, N. T. & Maezono, R. Size dependence of the bulk modulus of semiconductor nanocrystals from first-principles calculations. *Phys. Rev. B* **82**, 235321 (2010). URL <https://link.aps.org/doi/10.1103/PhysRevB.82.235321>.
16. Mori, Y., Kawarada, H. & Hiraki, A. Properties of metal/diamond interfaces and effects of oxygen adsorbed onto diamond surface. *Appl. Phys. Lett.* **58**, 940–941 (1991). URL <http://scitation.aip.org/content/aip/journal/apl/58/9/10.1063/1.104484>.
17. Kawarada, H. Hydrogen-terminated diamond surfaces and interfaces. *Surf. Sci. Rep.* **26**, 205 – 259 (1996). URL <http://www.sciencedirect.com/science/article/pii/S0167572997800027>.
18. Pickett, W. E. Thin superlattices and band-gap discontinuities: The (110) diamond - boron nitride interface. *Phys. Rev. B* **38**, 1316–1322 (1988). URL <http://link.aps.org/doi/10.1103/PhysRevB.38.1316>.
19. Lambrecht, W. R. L. & Segall, B. Electronic structure of (diamond c)/(sphalerite bn) (110) interfaces and superlattices. *Phys. Rev. B* **40**, 9909–9919 (1989). URL <http://link.aps.org/doi/10.1103/PhysRevB.40.9909>.
20. Erwin, S. C. & Pickett, W. E. Diamond-nickel interfaces: calculation of the electronic and atomic structure and schottky barriers. *Surf. Coat. Technol.* **47**, 487 – 495 (1991). URL <http://www.sciencedirect.com/science/article/pii/025789729190315N>.
21. Wang, X.-G. & Smith, J. R. Copper/diamond adhesion and hydrogen termination. *Phys. Rev. Lett.* **87**, 186103 (2001). URL <http://link.aps.org/doi/10.1103/PhysRevLett.87.186103>.
22. Qi, Y. & Hector, L. G. Hydrogen effect on adhesion and adhesive transfer at aluminum/diamond interfaces. *Phys. Rev. B* **68**, 201403 (2003). URL <http://link.aps.org/doi/10.1103/PhysRevB.68.201403>.
23. Qi, Y. & Hector, L. G. Adhesion and adhesive transfer at aluminum/diamond interfaces: A first-principles study. *Phys. Rev. B* **69**, 235401 (2004). URL <http://link.aps.org/doi/10.1103/PhysRevB.69.235401>.
24. Jia, Y., Zhu, W., Wang, E. G., Huo, Y. & Zhang, Z. Initial stages of ti growth on diamond (100) surfaces: From single adatom diffusion to quantum wire formation. *Phys. Rev. Lett.* **94**, 086101 (2005). URL <http://link.aps.org/doi/10.1103/PhysRevLett.94.086101>.
25. Guo, H., Qi, Y. & Li, X. Adhesion at diamond/metal interfaces: A density functional theory study. *J. Appl. Phys.* **10** (2010). URL <http://scitation.aip.org/content/aip/journal/jap/107/3/10.1063/1.3277013>.
26. Motochi, I. T., Makau, N. W. & Amolo, G. O. Metal-semiconductor ohmic contacts: An ab initio density functional theory study of the structural and electronic properties of metal-diamond (111)-(1 × 1) interfaces. *Diamond Relat. Mater.* **23**, 10 – 17 (2012). URL <http://www.sciencedirect.com/science/article/pii/S0925963511003980>.
27. Tiwari, A. K. *et al.* Electronic and structural properties of diamond (001) surfaces terminated by selected transition metals. *Phys. Rev. B* **86**, 155301 (2012). URL <http://link.aps.org/doi/10.1103/PhysRevB.86.155301>.
28. Monachon, C., Schusteritsch, G., Kaxiras, E. & Weber, L. Qualitative link between work of adhesion and thermal conductance of metal/diamond interfaces. *J. Appl. Phys.* **115** (2014). URL <http://scitation.aip.org/content/aip/journal/jap/115/12/10.1063/1.4869668>.

29. van der Weide, J. & Nemanich, R. J. Influence of interfacial hydrogen and oxygen on the schottky barrier height of nickel on (111) and (100) diamond surfaces. *Phys. Rev. B* **49**, 13629–13637 (1994). URL <http://link.aps.org/doi/10.1103/PhysRevB.49.13629>.
30. Giannozzi, P. *et al.* Quantum espresso: a modular and open-source software project for quantum simulations of materials. *J. Phys.: Condens. Matter* **21**, 395502 (2009). URL <http://stacks.iop.org/0953-8984/21/i=39/a=395502>.
31. Perdew, J. P., Burke, K. & Ernzerhof, M. Generalized gradient approximation made simple [phys. rev. lett. 77, 3865 (1996)]. *Phys. Rev. Lett.* **78**, 1396–1396 (1997). URL <http://link.aps.org/doi/10.1103/PhysRevLett.78.1396>.
32. Pickard, C. J. & Payne, M. C. Second-order $k \cdot p$ perturbation theory with vanderbilt pseudopotentials and plane waves. *Phys. Rev. B* **62**, 4383–4388 (2000). URL <http://link.aps.org/doi/10.1103/PhysRevB.62.4383>.
33. Marzari, N., Vanderbilt, D., De Vita, A. & Payne, M. C. Thermal contraction and disordering of the al(110) surface. *Phys. Rev. Lett.* **82**, 3296–3299 (1999). URL <http://link.aps.org/doi/10.1103/PhysRevLett.82.3296>.
34. Yan, Y., Zhang, S. B. & Al-Jassim, M. M. Graphite-like surface reconstructions on c111 and their implication for n -type diamond. *Phys. Rev. B* **66**, 201401 (2002). URL <http://link.aps.org/doi/10.1103/PhysRevB.66.201401>.
35. Erwin, S. C. & Pickett, W. E. Diamond-nickel interfaces: calculation of the electronic and atomic structure and schottky barriers. *Surf. Coat. Technol.* **47**, 487 – 495 (1991). URL <http://www.sciencedirect.com/science/article/pii/025789729190315N>.
36. Cordero, B. *et al.* Covalent radii revisited. *Dalton Trans.* 2832–2838 (2008). URL <http://dx.doi.org/10.1039/B801115J>.
37. Hongo, K. *et al.* Interpretation of hund’s multiplicity rule for the carbon atom. *The Journal of Chemical Physics* **121**, 7144–7147 (2004). URL <http://dx.doi.org/10.1063/1.1795151>.
38. Pickett, W. E. & Erwin, S. C. Electronic structure of an ideal diamond-nickel (001) interface. *Phys. Rev. B* **41**, 9756–9765 (1990). URL <http://link.aps.org/doi/10.1103/PhysRevB.41.9756>.
39. Himpsel, F. J., Eastman, D. E., Heimann, P. & van der Veen, J. F. Surface states on reconstructed diamond (111). *Phys. Rev. B* **24**, 7270–7274 (1981). URL <http://link.aps.org/doi/10.1103/PhysRevB.24.7270>.
40. Heine, V. Theory of surface states. *Phys. Rev.* **138**, A1689–A1696 (1965). URL <https://link.aps.org/doi/10.1103/PhysRev.138.A1689>.
41. Tersoff, J. Theory of semiconductor heterojunctions: The role of quantum dipoles. *Phys. Rev. B* **30**, 4874–4877 (1984). URL <https://link.aps.org/doi/10.1103/PhysRevB.30.4874>.
42. Birch, F. Finite elastic strain of cubic crystals. *Phys. Rev.* **71**, 809–824 (1947). URL <https://link.aps.org/doi/10.1103/PhysRev.71.809>.